28. Chouhan, S., Sharma, K. and Guleria, S., Antimicrobial activity of some essential oils – present status and future perspectives. *Medicines* (*Basel*), 2017, **4**, 58.
29. Li, Y., Nie, Y., Zhou, L., Li, S., Tang, X., Ding, Y. and Li, S., The possible mechanism of antifungal activity of cinnamon oil against *Rhizopus nigricans*. *J. Chem. Pharm. Res*., 2014, **6**, 12–20.
30. Wang, S. Y., Chen, P. F. and Chang, S. T., Antifungal activities of essential oils and their constituents from indigenous cinnamon (*Cinnamomum osmophloeum*) leaves against wood decay fungi. *Bioresour. Technol*., 2005, **96**, 813–818.
31. Cheng, S. S., Liu, J. Y., Chang, E. H. and Chang, S. T., Antifungal activity of cinnamaldehyde and eugenol congeners against wood-rot fungi. *Bioresour. Technol*., 2008, **99**, 5145–5149.
32. Xie, Y., Yang, Z., Cao, D., Rong, F., Ding, H. and Zhang, D., Antitermitic and antifungal activities of eugenol and its congeners from the flower buds of *Syzgium aromaticum* (clove). *Ind. Crops Prod*., 2015, **77**, 780–786.
33. Zhang, Z., Yang, T., Mi, N., Wang, Y., Li, G., Wang, L. and Xie, Y., Antifungal activity of monoterpenes against wood white-rot fungi. *Int. Biodeterior. Biodegrad*., 2016, **106**, 157–160.
34. Cheng, S. S., Chung, M. J., Lin, C. Y., Wang, Y. N. and Chang, S. T., Phytochemicals from *Cunninghamia konishii* Hayata act as antifungal agents. *J. Agric. Food. Chem*., 2011, **60**, 124–128.
35. Gill, A. O. and Holley, R. A., Mechanisms of bactericidal action of cinnamaldehyde against *Listeria monocytogenes* and of eugenol against *L. monocytogenes* and *Lactobacillus sakei*. *Appl. Environ. Microbiol*., 2004, **70**, 5750–5755.
36. de Almeida, R. R., Souto, R. N., Bastos, C. N., da Silva, M. H. and Maia, J. G., Chemical variation in *Piper aduncum* and biological properties of its dillapiole-rich essential oil. *Chem. Biodivers*., 2009, **6**, 1427–1434.
37. Bang, K. H., Lee, D. W., Park, H. M. and Rhee, Y. H., Inhibition of fungal cell wall synthesizing enzymes by trans-cinnamaldehyde. *Biosci. Biotechnol. Biochem*., 2000, **64**, 1061–1063.
38. Wang, C., Zhang, J., Chen, H., Fan, Y. and Shi, Z., Antifungal activity of eugenol against *Botrytis cinerea*. *Trop. Plant Pathol*., 2010, **35**, 137–143.
39. Asdadi, A. *et al.*, Study on chemical analysis, antioxidant and *in vitro* antifungal activities of essential oil from wild *Vitex agnus-castus* L. seeds growing in area of Argan Tree of Morocco against clinical strains of *Candida* responsible for nosocomial infections. *J. Mycol. Med*., 2015, **25**, e118–e127.
40. Pereira, F. G., Marquete, R., Domingos, L. T., Rocha, M. E., Ferreira-Pereira, A., Mansur, E. and Moreira, D. L., Antifungal activities of the essential oil and its fractions rich in sesquiterpenes from leaves of *Casearia sylvestris* Sw. *An. Acad. Bras. Ciênc*., 2017, **89**, 2817–2824.

ACKNOWLEDGEMENT. We extend our appreciation to the Deanship of Scientific Research at King Saud University for funding this work through Research Group No. (RGP-1440-094).

Received 9 July 2019; revised accepted 26 November 2019

doi: 10.18520/cs/v118/i5/796-801

First record of circa 970 Ma post-collisional A-type magmatism in the Sendra Granitoid Suite, central Aravalli orogen, northwest India

Jaideep K. Tiwana, Parampreet Kaur*, Naveen Chaudhri and Manisha

Centre of Advanced Study in Geology, Panjab University, Chandigarh 160 014, India

This study provides the first record for the emplacement of post-collisional A-type granites in extensional regime during the late Grenvillian period in northwest India. The ca. 970 Ma granites of the Sendra Granitoid Suite (Chang pluton) intrude calc-silicate rocks of the South Delhi Supergroup in the central Aravalli orogen. The Chang pluton is composed of granite *sensu stricto*; the granites are metaluminous, ferroan, calc-alkalic, and are characterized by high Ga/Al (>2.5), Nb + Y (>60 ppm), Ta + Yb (>6 ppm), REE, HFSE and zircon saturation temperatures, typical of A-type granites. The Y/Nb >1.2 further classified the rocks as A_2-subtype, signifying their derivation from crustal sources in a post-collisional setting. The crustal source is also supported by their high LILE (Rb, K and Ba), and Pb, Th and REE. The geochronological data and tectonics of the region indicate that the granites were emplaced about 30 Myr after the Grenvillian collisional orogeny. This scenario likely resulted due to delamination of the lower part of the thickened orogenic lithosphere. These results are expected to have significant implications for the assembly tectonics of the Rodinia supercontinent.

Keywords: A-type granites, post-collisional extension, whole-rock geochemistry, magmatism.

THERE is a broad consensus that the amalgamation of the Rodinia supercontinent took place between 1300 and 900 Ma (refs 1 and 2). The position of India in Rodinia, however, remains enigmatic. Some consider that India was not a part of Rodinia[3], while others are of the view that India was located west of Australia[4]. Further, it has also been proposed that the Eastern Ghats Mobile Belt (India) and the Rayner Province (East Antarctica) were attached by 990–900 Ma, and India broke away from Rodinia by 750 Ma (ref. 1). Like the Central Indian Tectonic Zone (CITZ) in central India, the northern and central parts of the Aravalli orogen (northwest India) also show imprints of the Grenvillian orogeny at 1085–930 Ma (refs 5 and 6).

In the central Aravalli orogen, the region about 10 km south of Beawar (Figure 1) experienced the late Grenvillian

*For correspondence. (e-mail: param.geol@gmail.com)

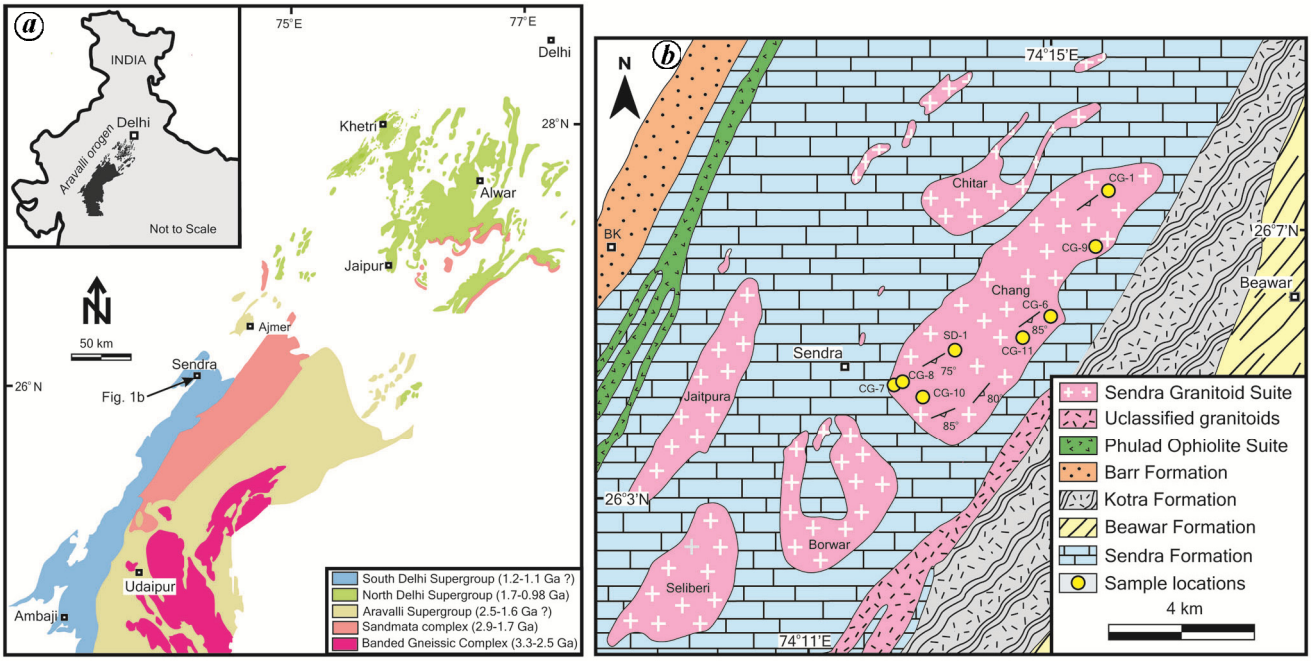

Figure 1. ***a***, Simplified regional geological map of the Aravalli orogen showing location of study area within the South Delhi Supergroup (Kaur *et al.*[42,43] and references therein). (Inset) Location of Aravalli orogen in NW India. ***b***, Geological map of the Sendra Granitoid Suite showing major lithological units and sample locations (modified after Gupta *et al.*[14]). BK, Birantiya Khurd.

felsic magmatism at 990–970 Ma (refs 7 and 8) in the Sendra Granitoid Suite. The present study provides detailed geochemical characterization of the Chang pluton of the Sendra Granitoid Suite, and challenges the current understanding by showing that the rocks are post-collisional A-type granites with no evidence of arc-related granitoids. These results could have significant implications to understand assembly tectonics of the Rodinia supercontinent.

The Aravalli orogen comprises of three major Precambrian stratigraphic units, the Palaeo- to Neoarchean Aravalli Banded Gneissic Complex[9] (3310–2485 Ma), which is succeeded by two supracrustal units, the Palaeoproterozoic Aravalli Supergroup and the Palaeo- to Mesoproterozoic Delhi Supergroup. The rocks of latter are deposited in two distinct sedimentary basins; north of Ajmer, they show older depositional ages between 1700 and 1000 Ma (the North Delhi Supergroup), and younger depositional ages (1200–1000 Ma; the South Delhi Supergroup) to the south of Ajmer[10,11].

Gupta *et al.*[12] divided the rocks of South Delhi Supergroup into an older Gogunda Group and a younger Kumbhalgarh Group. The Gogunda Group is dominantly arenaceous comprising conglomerate, quartzite, phyllite and calc-silicate rocks and is considered equivalent to the Alwar Group of the North Delhi Supergroup. The rocks of Kumbhalgarh Group are mostly calcareous with minor argillaceous and arenaceous metasedimentary rocks and are equated with the Ajabgarh Group of the North Delhi Supergroup. On the basis of lithological homogeneity, strike continuity and local relationship of superposition, rocks of the Gogunda Group are subdivided into three formations (Richer, Antalia and Kelwara), whereas those of the Kumbhalgarh Group into eight formations (Todgarh, Sendra, Beawar, Kotra, Barr, Kalakot, Ras and Basantgarh)[12]. The latter formations do not always show correct order of superposition due to superposed deformation and gradational or interfingering relationship of the lithounits[13].

The Sendra Formation of the Kumbhalgarh Group is of interest in this study (Figure 1). It is sandwiched between the rocks of Beawar and Kotra formations in the east and Barr Formation in the west. This lithounit with NE-SW trend, comprising predominantly calc-silicate rocks with minor bands of schist, quartzite and mafic magmatic rocks, is about 10–12 km thick in the northern part and narrows down to only a few metres in the south[13]. The calc-silicate rocks are intruded by a number of plutons of the Sendra Granitoid Suite, such as Chitar, Chang, Seliberi, Borwar and Jaitpura. It is pertinent to mention that no detailed modern geochemical studies have been made to characterize these granitoids.

The Chang pluton is the largest among these, covering more than 15 sq. km area in and around the Chang Reserve Forest. The granitoids show a sharp contact and an intrusive relation with the calc-silicate rocks of the Sendra Formation (Figure 2 *a*), as also previously reported by Agrawal and Srivastava[14]. Mafic dykes, pegmatites and quartz veins are the late intrusions, and xenoliths of calc-silicate rocks and mafic microgranular enclaves (MMEs)

Figure 2. Representative field and photomicrographs of the Chang pluton, illustrating (***a***) a sharp and intrusive contact between the Chang granites and the host calc-silicate rocks; (***b***) Chang granite showing well-developed foliation defined by biotite and amphibole and (***c***) overall view of the Chang granite illustrating a typical hypidiomorphic–granular texture (cross nicols).

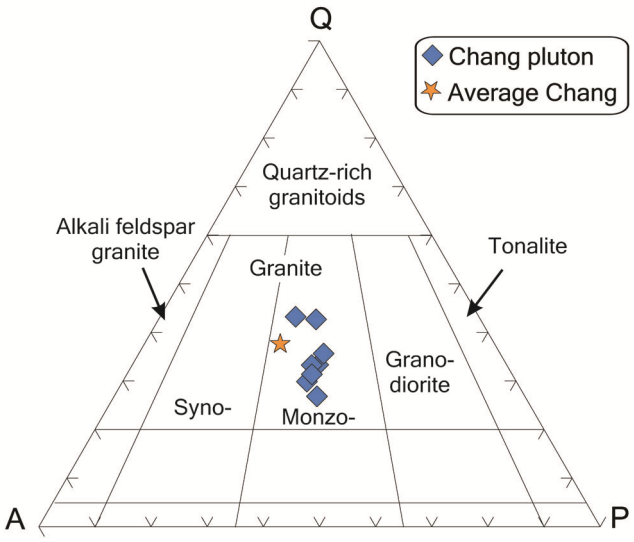

Figure 3. Modal compositions of the Chang granites in the QAP classification diagram of Streckeisen[44]. Average Chang = average modal data from Agrawal and Srivastava[14].

are common. The granitoids and country rocks show three sets of deformation structures. The former is interpreted to be of late syntectonic emplacement relative to D_2 phase of deformation and shows a complex deformational history[15,16]. The zircon U–Pb thermal ionization mass spectrometer (TIMS) data suggest the crystallization age of the Chang pluton at ca. 970 Ma (ref. 8).

The rocks of the intrusion are characterized by grey to pink-coloured, mostly medium grained, foliated and equigranular granitoids (Figure 2 *b*); rarely is it porphyritic. The foliation is well-defined by biotite and sometimes by biotite and amphibole. The rocks show typical subhedral–granular texture (Figure 2 *c*); they are subsolvus, containing magmatic K-feldspar and plagioclase. Essential minerals are quartz, K-feldspar, plagioclase, biotite and amphibole (Table 1). Accessory minerals constitute zircon, monazite, epidote, apatite, titanite, allanite, fluorite, iron oxides and secondary muscovite. The published mineral chemical data of two granitoid samples of the Chang pluton indicate that the plagioclase is albite to oligoclase ($An_{2.9}$ to $An_{19.2}$) and biotite is annite[8]. In the QAP ternary plot based on mode, the Chang samples are classified as granite *sensu stricto* (Figure 3).

Whole-rock geochemical data of the Chang pluton (Table 1) were analysed at the Activation Laboratories Ltd, Ontario, Canada. Details of sample preparation are given in Kaur *et al.*[10] and those of analytical protocol are mentioned elsewhere[17] (also see www.actlabs.com). The total rare earth element (REE) contents in the Chang granites are high (Table 1). Overall, the REE patterns are similar and moderately fractionated ($(La/Yb)_N$ = 2.7–4.3); Figure 4 *a*). All the samples show flat, heavy (H) REE patterns ($(Gd/Yb)_N$ = 0.9–1.2)) and strong negative Eu anomalies (Eu/Eu* = 0.26–0.43). In the primitive-mantle normalized multielement plot (Figure 4 *b*), the granites show prominent negative anomalies for Ba, Sr–Eu, P, Nb and Ti, which are likely to be related to fractionation of K-feldspar–biotite, plagioclase, apatite, rutile and titanite respectively. Importantly, these multielement patterns do not show any decoupling between the large-ion lithophile elements (LILEs) and high-field strength elements (HFSEs), which is typical of subduction-related magmatism.

The values of aluminium saturation index (ASI) index are less than 1, classifying the granites as metaluminous (Table 1). These granites are typically A-type as they are ferroan (high Fe-number (FeOt/(FeOt + MgO) = 0.90 to 0.97), calc-alkalic and exhibit high concentrations of Zr, Nb, Y, REE and Ga/Al (>2.5) compared to I-, S- and M-type granites[18–20] (Figure 5). They are high-temperature granites as indicated by zircon-saturation temperatures[21], which are higher than 832° ± 17°C (Table 1), well within the range of melt temperatures estimated experimentally for A-type magmas[22,23]. There exists a possibility that some A-type granites may represent highly fractionated I-type magmas[18]. In such a scenario, the enrichment of

Table 1. Representative whole-rock chemical and modal compositions for the Chang pluton, Sendra Granitoid Complex, Aravalli orogen, northwest India

Sample no.	CG-1	CG-6	CG-7	CG-8	CG-9	CG-10	CG-11	SD-1
SiO_2 (wt%)	72.2	77.0	74.2	72.7	76.8	72.3	76.2	77.0
TiO_2	0.30	0.18	0.26	0.30	0.14	0.30	0.17	0.18
Al_2O_3	12.76	11.91	12.35	13.07	12.09	12.88	11.99	11.91
$Fe_2O_3^t$	2.93	1.85	2.65	2.88	1.58	2.83	1.82	1.85
MnO	0.05	0.03	0.04	0.04	0.03	0.05	0.03	0.03
MgO	0.22	0.09	0.20	0.30	0.08	0.31	0.09	0.09
CaO	1.38	0.85	1.22	1.49	0.78	1.57	0.81	0.85
Na_2O	3.21	3.01	3.18	3.38	3.13	3.47	3.08	3.01
K_2O	5.08	5.18	4.91	4.74	5.24	4.44	5.14	5.18
P_2O_5	0.04	0.00	0.04	0.05	0.02	0.05	0.00	0.00
LOI	0.54	0.56	0.81	0.57	0.57	0.51	0.49	0.56
Sum	98.7	100.6	99.9	99.5	100.4	98.7	99.8	100.6
Sc (ppm)	6	4	6	6	5	6	5	6
V	11	6	9	11	6	14	6	11
Cr	<20	30	30	<20	30	<20	30	<20
Co	19	21	22	20	26	21	22	21
Ni	<20	<20	<20	<20	<20	<20	<20	<20
Zn	70	50	60	50	40	50	60	60
Ga	21	23	23	19	24	18	23	20
Rb	264	282	290	254	310	231	288	244
Sr	50	41	46	53	32	57	33	53
Y	120	126	120	79	126	92	123	115
Zr	351	257	356	317	201	270	235	344
Nb	19	12	19	12	24	15	17	18
Ba	807	584	679	655	466	619	505	781
Pb	28	27	27	23	33	26	48	26
Th	27.7	30.2	33	27.4	43.2	26.5	33.2	26.8
U	4.2	4.4	4.9	4.7	7	2.6	8.7	3.4
Hf	8.3	7.5	10.3	7.3	7.5	6.4	7.5	8.3
Ta	2.2	2.1	2.7	1.5	3.8	1.8	2.8	2.0
La	76.1	69.2	71.3	53.1	56.6	57.2	65.6	76.8
Ce	159	147	150	111	120	120	137	160
Pr	18.2	16.8	17.2	12.3	13.9	13.5	15.6	18.5
Nd	70.7	62.6	66.3	46.7	54.4	52.7	60.9	71.1
Sm	16.3	15.3	15.4	10.9	13.7	12.1	14.3	16.5
Eu	2.13	1.51	1.96	1.57	1.21	1.66	1.35	2.17
Gd	17.2	16.3	16.8	11.5	15.2	12.6	15.5	17.3
Tb	2.9	3.2	3.1	1.9	3	2.2	3	2.9
Dy	19.1	20.5	19.9	12.6	19.5	14.3	19.7	18.9
Ho	3.9	4.5	4.2	2.6	4.2	3	4.1	3.8
Er	11.9	13.1	12.5	7.9	13.1	9.1	12.5	11.5
Tm	1.83	2.05	1.95	1.22	2.09	1.43	1.96	1.72
Yb	12.5	13.4	13	8.4	14.5	9.7	13.2	11.6
Lu	1.86	2.02	2.09	1.29	2.24	1.52	1.97	1.75
∑REE	424.12	397.08	408.7	291.78	344.94	319.21	376.98	424.84
$(La/Yb)_N$	4.1	3.5	3.7	4.3	2.7	4.0	3.4	2.9
$(La/Sm)_N$	2.9	2.8	2.9	3.0	2.6	3.0	2.9	4.5
$(Gd/Yb)_N$	1.1	1.0	1.0	1.1	0.9	1.1	1.0	1.2
Eu/Eu*	0.39	0.29	0.37	0.43	0.26	0.41	0.28	0.39
ASI	0.97	0.98	0.97	0.98	0.99	0.97	0.99	0.96
$10^4 \times Ga/Al$	3.11	2.86	3.06	3.33	3.59	2.79	3.78	2.74
ZrnT°C	849	828	855	842	806	825	821	848
Nb + Y	139	138	139	91	150	107	140	133
Ta + Yb	14.7	15.5	15.7	9.9	18.3	11.5	16	13.6
Modal%								
Quartz	28.3	31.4	27.3	27.8	34.0	27.1	40.1	37.9
K-feldspar	28.5	32.8	34.1	31.6	30.0	37.4	30.3	26.0
Plagioclase	28.1	30.2	30.0	29.2	31.4	35.5	22.4	24.9
Biotite	12.3	4.2	6.3	5.8	4.2	6.0	5.7	9.2
Amphibole	1.7	–	–	3.8	–	2.9	–	0.3
Acc. Min.	1.0	1.4	2.3	1.8	0.4	1.4	1.5	1.7

Eu/Eu* = $Eu_N/(Sm_N \times Gd_N)^{½}$, ASI, Molar $Al_2O_3/(CaO\text{-}3.3P_2O_5 + Na_2O + K_2O)$. Zrn, Zircon; Acc. Min., Accessory minerals, which include zircon, monazite, apatite, epidote, titanite, allanite, fluorite, iron oxides and secondary muscovite.

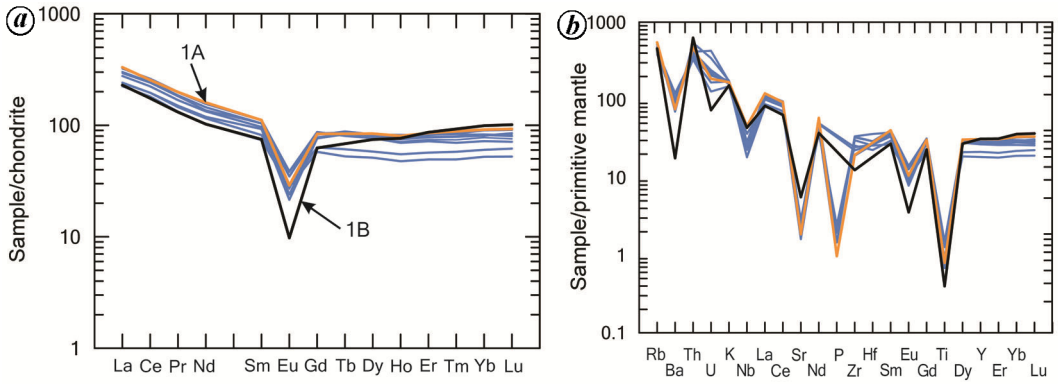

Figure 4. (***a***) Chondrite-normalized REE and (***b***) primitive-mantle normalized multi-element diagrams for the granites of Chang pluton. The normalizing values in both the diagrams are after McDonough and Sun[45]. Data for samples 1A (LC99I-1A) and 1B (LC99I-1B) are from Pandit *et al.*[8].

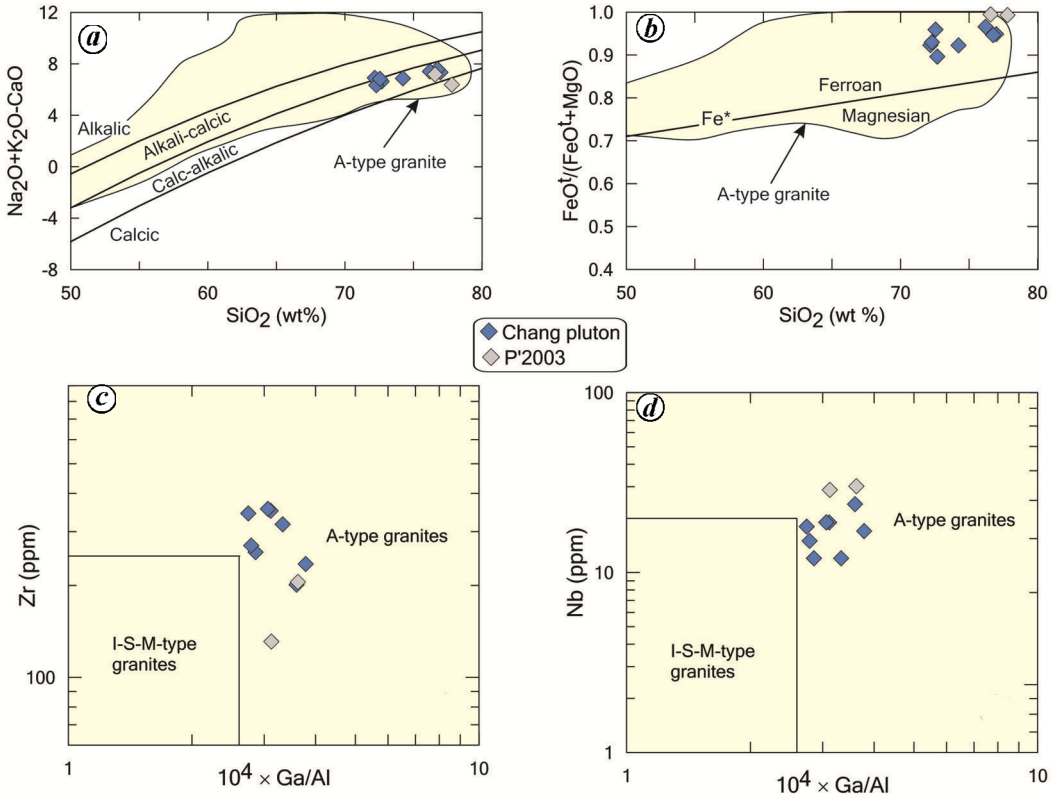

Figure 5. Whole-rock chemical composition of the Chang granites in the discrimination diagrams: (***a***) modified alkali–lime index ($Na_2O + K_2O$–CaO in wt%) versus SiO_2 (wt%; ref. 20), (***b***) $FeO^t/(FeOt + MgO)$ versus SiO_2 (wt%; ref. 20). The Fe-number (Fe*) dividing line is after Frost and Frost[46], (***c***) Zr (ppm) versus $10^4 \times Ga/Al$ (ref. 18) and (***d***) Nb (ppm) versus $10^4 \times Ga/Al$ (ref. 18). P′2003, data from Pandit *et al.*[8].

Nb and Y will be a function of the degree of fractional crystallization[18,24]. Also, the fractionated I-type granites will show lower zircon saturation temperatures (<800°C) due to lower Zr contents than the A-type granites[24,25]. By contrast, Nb and Y do not exhibit any trend with fractionation (increasing SiO_2 content) in the studied granites, and also the zircon saturation temperatures are high (Table 1), which is typical for A-type granites.

Recently, Whalen and Hilderbrand[26] using modern trace element data compilation, proposed new tectonic discrimination plots for granitoids and also modified the older diagrams of Pearce *et al.*[27]. These workers have demonstrated that A-type granites can be easily distinguished from arc-related and slab failure granitoids based on Nb + Y > 60 ppm and Ta + Yb > 6 ppm. In all the granites under study, Nb + Y values are 91–150 ppm and

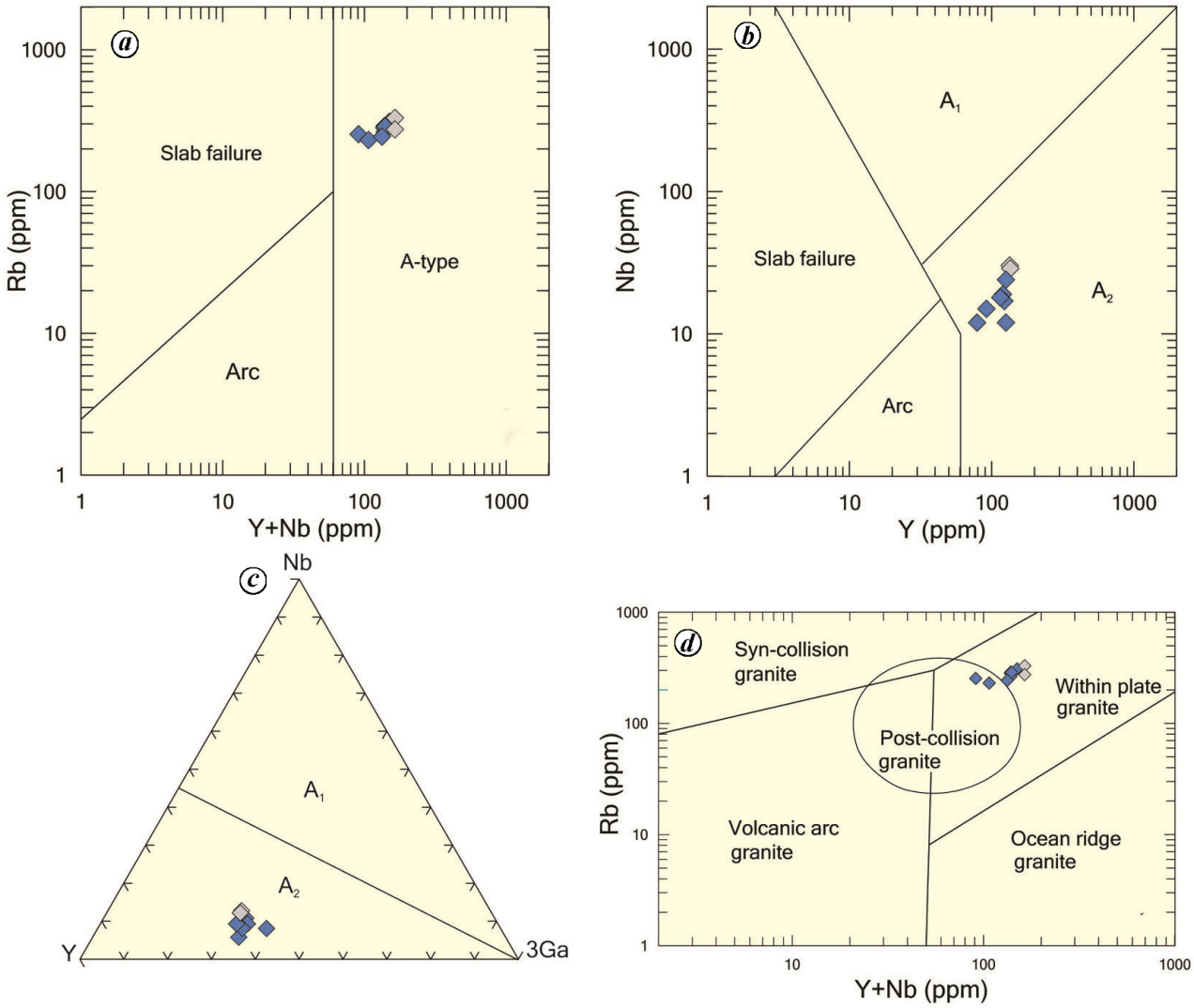

Figure 6. ***a***, Modified (Pearce *et al.*[27]) Rb versus Y + Nb tectonic discrimination diagram[26]; ***b***, modified (Pearce *et al.*[27]) Nb versus Y tectonic discrimination diagram[26]; ***c***, Y–Nb–3Ga ternary discrimination diagram of Eby[28]; ***d***, Rb (ppm) versus Y + Nb (ppm) tectonic discrimination diagram[27]. Field of post-collision granite is after Pearce[29]. Symbol explanation as in Figure 5.

those of Ta + Yb between 9.9 and 18.3 ppm (Table 1), indicating that the rocks are not arc-related granitoids. Furthermore, in the modified Rb versus Nb + Y plot of Pearce *et al.*[27], the rocks cluster distinctly in the A-type granite field, away from arc-related granitoids (Figure 6 *a*). The Nb versus Y plot also suggests that these are A_2-subtype granites (Figure 6 *b*), which is also confirmed in the Y–Nb–3Ga discrimination diagram of Eby[28], as the granites form a tight cluster in the A_2 field because they have Y/Nb > 1.2 (Figure 6 *c*). Such granites are thought to be generated from subcontinental lithosphere or lower continental crust in post-collisional or post-orogenic settings, perhaps during late-stage extensional collapse[26,28]. In the Rb versus Y + Nb discrimination diagram (Figure 6 *d*), the granites fall either in the post-collisional field or close to it[29]. Nevertheless, some samples with relatively high Y values plot outside the post-collisional field, which may be attributed to their magma generation by relatively lower degree of partial melting[30].

In summary, the ca. 970 Ma A_2-subtype granites of the Sendra Granitoid Suite were emplaced in a post-collisional extensional realm, perhaps during the late stages of collision[26]. Bhowmik *et al.*[5] constrained the timing of granulite facies metamorphism at 1.09–1.01 Ga in the Pilwa–Chinwali granulites, located ca. 80 km NE from Sendra at the northwestern margin of the Aravalli orogen. It has been advocated that the impact of ca. 1.0 Ga collisional orogenic front was prevalent almost along the entire length of the Aravalli orogen[31]. In view of this, a post-collisional setting seems to be consistent with the available geochronological data of the Chang pluton (970 Ma) that intruded the rocks of the South Delhi Supergroup about 30 Myr after the collisional orogeny. This post-collisional magmatism likely resulted from

delamination of the lower part of the thickened orogenic lithosphere leading to transition from compressional to extensional tectonic setting[32,33]. The upwelling mantle provided sufficient heat to induce melting of crust to produce A-type magmas.

It is noteworthy that the proposed tectonic setting of the Sendra granitoids is in contrast with the previous studies. For example, Pandit *et al.*[8], based on the metaluminous character of two granite samples, interpreted the Chang pluton of the Sendra Granitoid Suite in terms of I-type classification, whereas these two samples distinctly show an A-type affinity and also similar multielement patterns (Figures 4–6). These authors also suggested that the Chang pluton is an Andean-type intrusion representing the product of convergent margin processes. This interpretation was based on the age correlation between the Chang pluton (968 ± 1 Ma) and the Ranakpur diorite (1012 ± 78 Ma: Sm–Nd whole rock isochron[34]), located about 135 km SW of Sendra. The latter is considered to be chemically similar to the associated ocean arc basalts[34]. In this context, it is worth mentioning that Deb *et al.*[7] suggested an arc terrane between Ambaji in the south and Sendra in the north, known as the Ambaji–Sendra belt. Moreover, an arc-related tectonic setting for the volcanogenic massive sulphide (VMS) deposits in the southern domain of the belt has been interpreted on the basis of geochemical characterization of the mafic volcanics[35]. The tectonic setting for the VMS deposits in the northern domain at Birantiya Khurd (Figure 1 *b*) is, however, uncertain because Deb and Sarkar[35] considered these deposits to have formed by an analogous mechanism as those of Ambaji, in view of their similar geological setting. Based on the geochronologic and lithotectonic affinity between the VMS deposits of Ambaji and Birantiya Khurd, the arc-related rocks in the southern domain were suggested to extend till Sendra[7]. Thus, it is apparent that the proposed arc affinity for the rocks in the northern part of the Ambaji–Sendra belt is yet to be constrained by further detailed geological studies. It should be noted before this study, the granitoids throughout this belt virtually lack modern geochemical data, except for the two analyses available from the Chang pluton.

This study records the emplacement of post-collisional A-type Sendra granitoids within extensional encratonic environment. Furthermore, the age range of 990–970 Ma for these granitoids and the associated rhyolites corresponds to the assembly time span of the Rodinia supercontinent (1300–900 Ma). The rocks of A-type affinity during the Grenvillian magmatism have also been reported from many worldwide terranes; for example, southwestern Grenville province in Canada[32], northern Virginia[33], central Colorado[36], Laurentia, Texas and New Mexico[37,38], and southern Norway[39,40]. The present study, therefore, supports growing evidence that during the assembly of Rodinia, there was a relative lack of subduction-related arc magmatism in contrast to the arc-collisional magmatism prevalent during the assembly of other supercontinents, such as Columbia and Gondwana[41]. This contention, however, needs to be confirmed in India wherever the Grenvillian rocks are exposed. Therefore, revelation of 970 Ma A-type extensional-related Sendra granitoids invokes the need for more robust geochemical and geochronological constraints in order to explore the relative prevalence of extension/subduction-related magmatism during the Grenvillian processes in NW India. This may further have implications to refine the configuration of Rodinia in context of India's position.

1. Li, Z. X. *et al.*, Assembly, configuration, and break-up history of Rodinia: a synthesis. *Precambrian Res*., 2008, **160**, 179–210.
2. Bogdanova, S. V., Pisarevsky, S. A. and Li, Z. X., Assembly and breakup of Rodinia (some results of IGCP Project 440). *Stratigr. Geol. Corr*., 2009, **17**, 259–274.
3. Pisarevsky, S. A., Wingate, M. T. D., Powell, C. McA., Johnson, S. and Evans, D. A. D., Models of Rodinia assembly and fragmentation. In *Proterozoic East Gondwana: Supercontinent Assembly and Breakup* (eds Yoshida, M., Windley, B. F. and Dasgupta, S.), Geological Society London, Special Publication, 2003, vol. 206, pp. 35–55.
4. Torsvik, T. H., Carter, L. M., Ashwal, L. D., Bhushan, S. K., Pandit, M. K. and Jamtveit, B., Rodinia refined or obscured: palaeomagnetism of the Malani igneous suite (NW India). *Precambrian Res*., 2001, **108**, 319–333.
5. Bhowmik, S. K., Dasgupta, S., Baruah, S. and Kalita, D., Thermal history of a Late Mesoproterozoic paired metamorphic belt (?) during Rodinia assembly: new insights from medium-pressure granulites from the Aravalli–Delhi Mobile Belt, northwestern India. *Geosci. Front*., 2018, **9**, 335–354.
6. Bhowmik, S. K., The current status of orogenesis in the Central Indian Tectonic Zone: a review from its southern margin. *Geol. J*., 2019, **54**, 2912–2934.
7. Deb, M., Thorpe, R. I., Krstic, D., Corfu, F. and Davis, D. W., Zircon U–Pb and galena Pb isotope evidence for an approximate 1.0 Ga terrane constituting the western margin of the Aravalli–Delhi orogenic belt, northwestern India. *Precambrian Res*., 2001, **108**, 195–213.
8. Pandit, M. K., Carter, L. M., Ashwal, L. D., Tucker, R. D., Torsvik, T. H., Jamtveit, B. and Bhushan, S. K., Age, petrogenesis and significance of 1 Ga granitoids and related rocks from the Sendra area, Aravalli craton, NW India. *J. Asian Earth Sci*., 2003, **22**, 363–381.
9. Kaur, P., Zeh, A. and Chaudhri, N., Archean crustal evolution of the Aravalli Banded Gneissic Complex, NW India: constraints from zircon U–Pb ages, Lu–Hf isotope systematics, and whole-rock geochemistry. *Precambrian Res*., 2019, **327**, 81–102.
10. Kaur, P., Zeh, A., Chaudhri, N., Gerdes, A. and Okrusch, M., Archaean to Palaeoproterozoic crustal evolution of the Aravalli orogen, NW India, and its hinterland: the U–Pb and Hf isotope record of detrital zircon. *Precambrian Res*., 2011, **187**, 155–164.
11. McKenzie, N. R., Hughes, N. C., Myrow, P. M., Banerjee, D. M., Deb, M. and Planavsky, N. J., New age constraints for the Proterozoic Aravalli–Delhi successions of India and their implications. *Precambrian Res*., 2013, **238**, 120–128.
12. Gupta, S. N., Arora, Y. K., Mathur, R. K., Iqbaluddin, Prasad, B., Sahai, T. N. and Sharma, S. B., Lithostratigraphic map of Aravalli region, southern Rajasthan and northeastern Gujarat. Geological Survey of India Publication, Hyderabad, 1980.
13. Gupta, S. N., Arora, Y. K., Mathur, R. K., Iqbaluddin, Prasad, B., Sahai, T. N. and Sharma, S. B., The Precambrian geology of the

Aravalli region, southern Rajasthan and northeastern Gujarat. *Mem. Geol. Surv. India*, 1997, **123**, 262.
14. Agrawal, S. and Srivastava, R. K., Geochemistry of Late Proterozoic Sendra Granitoid Suite, Central Rajastahn, India: role of magma mixing/hybridization process in their genesis. *J. Geol. Soc. India*, 1997, **50**, 607–618.
15. Gangopadhyay, A. and Mukhopadhyay, D., Structural geometry of the Delhi Supergroup near Sendra – an example of the impress of granite diapirism on tectonic structures. *Rec. Res. Geol*., 1987, **13**, 45–60.
16. Tobisch, O. T., Collerson, K. D., Bhattacharyya, T. and Mukhopadhyay, D., Structural relationships and Sm–Nd isotope systematics of polymetamorphic granitic gneisses and granitic rocks from central Rajasthan, India: implications for the evolution of the Aravalli craton. *Precambrian Res*., 1994, **65**, 319–339.
17. Kaur, P., Chaudhri, N. and Eliyas, N., Origin of trondhjemite and albitite at the expense of A-type granite, Aravalli orogen, India: evidence from new metasoamtic replacement fronts. *Geosci. Front*., 2019, **10**, 1891–1913.
18. Whalen, J. B., Currie, K. L. and Chappell, B. W., A-type granites, geochemical characteristics, discrimination and petrogenesis. *Contrib. Mineral. Petrol*., 1987, **95**, 407–419.
19. Collins, W. J., Beams, S. D., White, A. J. R. and Chappell, B. W., Nature and origin of A-type granites with particular reference to southeastern Australia. *Contrib. Mineral. Petrol.*, 1982, **80**, 189–200.
20. Frost, B. R., Barnes, C. G., Collins, W. J., Arculus, R. J., Ellis, D. J. and Frost, C. D., A geochemical classification for granitic rocks. *J. Petrol*., 2001, **42**, 2033–2048.
21. Watson, E. B. and Harrison, T. M., Zircon saturation revisited: temperature and composition effects in a variety of crustal magmas types. *Earth Planet. Sci. Lett*., 1983, **64**, 295–304.
22. Clemens, J. D., Holloway, J. R. and White, A. J. R., Origin of an A-type granite: experimental constraints. *Am. Mineral*., 1986, **71**, 317–324.
23. Dall'Agnol, R., Scaillet, B. and Pichavant, M., An experimental study of a Lower Proetrozoic A-type granite from the Eastern Amazonian Craton, Brazil. *J. Petrol*., 1999, **40**, 1673–1698.
24. King, P. L., White, A. J. R., Chappell, B. W. and Allen, C. M., Characterization and origin of aluminous A-type granites from the Lachlan Fold Belt, southeastern Australia. *J. Petrol*., 1997, **38**, 371–391.
25. King, P. L., Chappell, B. W., Allen, C. M. and White, A. J. R., Are A-type granites the high-temperature felsic granites? Evidence from fractionated granites of the Wangrah Suite. *Aust. J. Earth Sci.*, 2001, **48**, 501–514.
26. Whalen, J. B. and Hilderbrand, R. S., Trace element discrimination of arc, slab failure, and A-type granitic rocks. *Lithos*, 2019, **348–349**, 105179.
27. Pearce, J. A., Harris, N. B. W. and Tindle, A. G., Trace element discrimination diagrams for the tectonic interpretation of granitic rocks. *J. Petrol*., 1984, **25**, 956–983.
28. Eby, G. N., Chemical subdivision of the A-type granitoids; petrogenetic and tectonic implications. *Geology*, 1992, **20**, 641–644.
29. Pearce, J. A., Sources and settings of granitic rocks. *Episodes*, 1996, **19**, 120–125.
30. Kaur, P., Zeh, A., Chaudhri, N. and Eliyas, N., Two distinct sources of 1.73–1.70 Ga A-type granites from the northern Aravalli orogen, NW India: constraints from in situ zircon U–Pb ages and Lu–Hf isotopes. *Gondwana Res*., 2017, **49**, 164–181.
31. Bhowmik, S. K., Bernhardt, H.-J. and Dasgupta, S., Grenvillian age high-pressure upper amphibolite–granulite metamorphism in the Aravalli–Delhi Mobile Belt, northwestern India: new evidence from monazite chemical age and its implication. *Precambrian Res*., 2010, **178**, 168–184.
32. Corrigan, D. and Hanmer, S., Anorthosite and related granitoids in the Grenville orogen: a product of convective thinning of the lithosphere? *Geology*, 1997, **25**, 61–64.
33. Tollo, R. P., Aleinikoff, J. N., Borduas, E. A., Dickin, A. P., McNutt, R. H. and Fanning, C. M., Grenvillian magmatism in the northern Virginia Blue Ridge: petrologic implications of episodic granitic magma production and the significance of postorogenic A-type charnockite. *Precambrian Res*., 2006, **151**, 224–264.
34. Volpe, A. M. and Macdougall, J. D., Geochemistry and isotopic characteristics of mafic (Phulad Ophiolite) and related rocks in the Delhi Supergroup, Rajasthan, India: implications for rifting in the Proterozoic. *Precambrian Res*., 1990, **48**, 167–191.
35. Deb, M. and Sarkar, S. C., Proterozoic tectonic evolution and metallogenesis in the Aravalli–Delhi orogenic complex, northwestern India. *Precambrian Res*., 1990, **46**, 115–137.
36. Smith, D. R. *et al.*, Petrology and geochemistry of late-stage intrusions of the A-type, mid-Proterozoic Pikes Peak batholith (central Colorado, USA): implications for petrogenetic models. *Precambrian Res*., 1999, **98**, 271–305.
37. Shannon, W. M., Barnes, C. G. and Bickford, M. E., Grenville magmatism in west Texas: petrology and geochemistry of Red Bluff granitic suite. *J. Petrol*., 1997, **38**, 1279–1305.
38. Li, Y., Barnes, M. A., Barnes, C. G. and Frost, C. D., Grenville-age A-type and related magmatism in southern Laurentia, Texas and New Mexico, USA. *Lithos*, 2007, **97**, 58–87.
39. Vander Auwera, J., Bogaerts, M., Liégeois, J.-P., Demaiffe, D. D., Wilmart, E., Bolle, O. and Duchesne, J. C., Derivation of 1.0–0.9 Ga ferro-potassic A-type granitoids of southern Norway by extreme differentiation from basic magmas. *Precambrian Res*., 2003, **124**, 107–148.
40. Bogaerts, M., Scaillet, B., Liégeois, J.-P. and Vander Auwera, J., Petrology and geochemistry of the Lyngdal granodiorite (Southern Norway) and the role of fractional crystallisation in the genesis of Proterozoic ferro-potassic A-type granites. *Precambrian Res*., 2003, **124**, 149–184.
41. Liu, C., Runyon, S. E., Knoll, A. H. and Hazen, R. M., The same and not the same: ore geology, mineralogy and geochemistry of Rodinia assembly versus other supercontinents. *Earth-Sci. Rev*., 2019, **196**, 102860.
42. Kaur, P., Chaudhri, N. and Hofmann, A. W., New evidence for two sharp replacement fronts during albitization of granitoids from northern Aravalli orogen, northwest India. *Int. Geol. Rev*., 2015, **57**, 1660–1685.
43. Kaur, P., Zeh, A. and Chaudhri, N., Palaeoproterozoic continental-arc magmatism, and Neoproterozoic metamorphism in the Aravalli–Delhi orogenic belt, NW India: new constraints from *in situ* zircon U–Pb–Hf isotope systematics, monazite U–Pb dating and whole-rock geochemistry. *J. Asian Earth Sci*., 2017, **136**, 68–88.
44. Streckeisen, A., To each plutonic rock its proper name. *Earth-Sci. Rev*., 1976, **12**, 1–33.
45. McDonough, W. F. and Sun, S.-S., Composition of the Earth. *Chem. Geol*., 1995, **120**, 223–253.
46. Frost, B. R. and Frost, C. D., A geochemical classification for feldspathic igneous rocks. *J. Petrol*., 2008, **49**, 1955–1969.

ACKNOWLEDGEMENTS. We thank the two anonymous reviewers, and the handling editor for their critical comments which helped improve the manuscript. The financial assistance provided by Ministry of Earth Sciences, New Delhi (MoES/P.O./(Geo)/100(2)/2017) is gratefully acknowledged.

Received 11 June 2019; revised accepted 7 November 2019

doi: 10.18520/cs/v118/i5/801-808